A Novel Optoelectronic System for Distortion-Invariant ATR

Contract No. N00014-93-C-0135

Period of Performance: 07/02/93 to 01/02/94

Final Report

Reporting Period: 07/02/93 to 02/01/94

Presented to:
Office of Naval Research
800 North Quincy Street
Arlington, VA 22217-5660

Technical Monitor
William Miceli

Original contains color plates: All DTIC reproductions will be in black and white.

Presented by:
Physical Optics Corporation
Research & Development Division
20600 Gramercy Place, Suite 103
Torrance, California 90501

Principal Investigator
Lev Sadovnik
(310) 320-3088

March 1994

Research supported by Strategic Defense Initiative/Innovative Science and Technology and managed by the Office of Naval Research

DISCLAIMER NOTICE

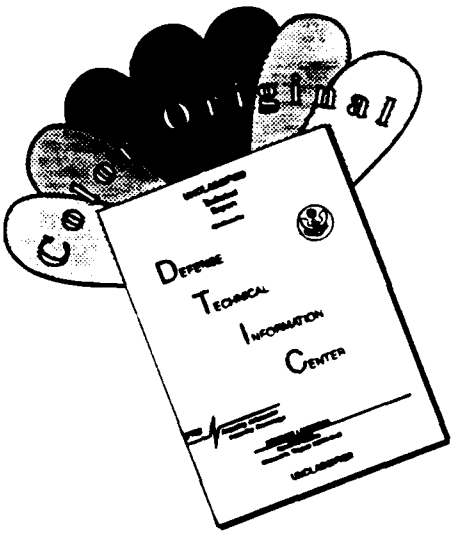

THIS DOCUMENT IS BEST QUALITY AVAILABLE. THE COPY FURNISHED TO DTIC CONTAINED A SIGNIFICANT NUMBER OF COLOR PAGES WHICH DO NOT REPRODUCE LEGIBLY ON BLACK AND WHITE MICROFICHE.

REPORT DOCUMENTATION PAGE

Form Approved
OMB No. 0704-0188

1. AGENCY USE ONLY *(Leave blank)*	2. REPORT DATE	3. REPORT TYPE AND DATES COVERED
	2-1-94	Final 7-2-93 through 2-1-94

4. TITLE AND SUBTITLE

A Novel Optoelectronic System for Distortion-Invariant ATR

5. FUNDING NUMBERS

C: N00014-93-C-0135

6. AUTHOR(S)

Lev Sadovnik

7. PERFORMING ORGANIZATION NAME(S) AND ADDRESS(ES)

Physical Optics Corporation
20600 Gramercy Place, Building 100
Torrance, California 90501

8. PERFORMING ORGANIZATION REPORT NUMBER

3225

9. SPONSORING / MONITORING AGENCY NAME(S) AND ADDRESS(ES)

Office of Naval Research
800 North Quincy Street
Arlington, VA 22217-0135

10. SPONSORING / MONITORING AGENCY REPORT NUMBER

11. SUPPLEMENTARY NOTES

12a. DISTRIBUTION / AVAILABILITY STATEMENT

Unlimited

12b. DISTRIBUTION CODE

13. ABSTRACT *(Maximum 200 words)*

The proposed idea is to enhance existing optical correlation based automatic target recognition (ATR) by introducing scale, translation, and rotation invariance (STRI). Previously, STRI was achieved by utilizing a library of matched filters corresponding to various positions of rotation and scale variation. We find that simple preprocessing can eliminate the need for the library since any STR changes in the input image can be nullified by bringing an input image to what we call its archetype.

Physical Optics Corporation's (POC's) new approach includes a segmentation preprocessor (required to select any potential object of interest in an image of a realistic scene), POC's invariant preprocessor, and a standard optical correlator. This combination will greatly increase recognition speed and will simplify the recognition training procedure since only one in-plane position of the target will be needed to provide STRI recognition.

The Phase I research described in this report opened a new approach to invariant ATR in which in-plane object position will no longer be of concern and, therefore, the best matched filter can be exploited to attain maximum confidence of identification. This should result in the development of hardware capable of operating in a real-time mode.

14. SUBJECT TERMS	15. NUMBER OF PAGES
Automatic Target Recognition	28
	16. PRICE CODE

17. SECURITY CLASSIFICATION OF REPORT	18. SECURITY CLASSIFICATION OF THIS PAGE	19. SECURITY CLASSIFICATION OF ABSTRACT	20. LIMITATION OF ABSTRACT
Unclassified	Unclassified	Unclassified	SAR

Executive Summary

In this report, we provide a theoretical proof and an experimental verification of a new approach to invariant automatic target recognition (ATR) proposed by Physical Optics Corporation (POC). The core of the concept is to determine the so-called archetype image for a class of all images derived from a given object through scale, translation and rotational (STR) changes. This archetype image will then represent the whole class of STR transformations and can be used for further identification. We started with a comparative analysis of the moments transformation which is the closest related approach. Next, we developed an algorithm for bringing an input image to its archetype position. We tested this algorithm in the presence of added noise and varying illumination. We also confirmed the robustness of the algorithm performance experimentally by using an optical correlator to classify the obtained archetype images. At the end of this report we outline the proposed ATR system development.

TABLE OF CONTENTS

LIST OF FIGURES AND TABLES

1.0 INTRODUCTION

The goal of this research is to develop a new concept of scale, translation, and rotation invariant optical processing for ATR. Research on invariant ATR has been underway for the last thirty to forty years, motivated by various military and commercial applications, the latter including on-line control, robotic vision and biomedical analysis (such as used in cytopathology). The general requirements for invariant ATR have been developed over the years and can be stated as:

- Invariant mapping of an input image onto a feature space
- Unique classification and/or identification.

A fully invariant system would perform ATR without regard to translation (shift), rotation, dilation (scale), and illumination or viewing angle. In this project, we limit our investigation to the first three invariant features only, although we suggest methods for incorporating the other two.

The principle of invariant ATR can be reduced to a block diagram shown in Figure 1-1. The transforms take the form of Fourier, Gabor, windowed, wavelet or some other integral transformations. Matching can be done either by using a prestored filter (matched filter) or a continuously updated (joint transform correlator) filter. Final identification is typically done by choosing some distance function in a feature space such as Euclidean, Mahalanobis, or minimum entropy.

Figure 1-1
Block diagram of ATR.

Figure 1-2 shows a hierarchy of images of increasing complexity, beginning with simple 2-D binary objects at the left and increasing in complexity to the right. The procedure illustrated in Figure 1-1 has not been fully successful for realistic 3-D objects whose increased image complexity can be described by Figure 1-2.

Figure 1-2
Image complexity string.

We propose to reduce the image complexity described in Figure 1-2 by following the steps in Figure 1-3 which correspond, box for box, to Figure 1-2.

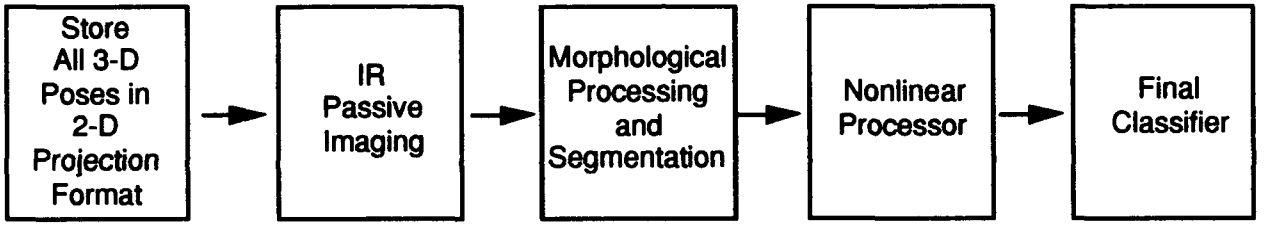

Figure 1-3
Reducing image complexity.

In Phase I, we concentrated on the nonlinear optical processing and electronic identifier stages, which correspond to the analysis of 2-D gray level objects (or 2-D projections of 3-D objects). The problem of variable illumination and shadowing can be overcome through the use of passive IR imaging. The problem of 3-D ATR includes out-of-plane rotations which constitute different objects and, thus, cannot be related to each other by any transformation unless full knowledge of the object is available. To identify an object from any of its projections, all of the possible projections must be stored as training patterns. This large memory storage requirement is reduced by the compression inherent in the proposed STRI processor.

2.0 PREVIOUS WORK ON INVARIANT PATTERN RECOGNITION

In this section, we describe advances made in STRI ATR to date.

Pattern recognition is of interest in many disciplines, since it can provide automatic recognition of signals and objects. Optical pattern recognition, in particular, will provide tools for machine vision, robotics, automation and image understanding, by taking advantage of the parallel processing capabilities of optics.

One of the main demands placed on a recognition system is that it be invariant to changes in input, i.e., that it enable object recognition or classification, even when the object is distorted due to changes in position, rotation or size.

Even digital ATR is a challenging task. There is no universal approach that can recognize targets in any circumstances. The key issue is the feature extraction that determines the pattern recognition. Human beings easily determine the most significant features of images. Machines may not be able to adaptively choose the feature extraction algorithm that is suitable to the circumstance.

We evaluated the performance of the following algorithms of invariant feature extraction and pattern recognition:

1. Orthogonal Fourier-Mellin Moments (OFMMs);
2. Fourier Descriptors (FDs);
3. Geometrical approach to multiple circular harmonic filters (CHFs);
4. Phase-only Synthetic Discriminate Function (SDF) filters;
5. Composite wavelet matched filters;
6. Fourier-Mellin Descriptors (FMDs);
7. Image normalization using low-order Fourier-Mellin moments;
8. Moment invariants;
9. Phase-only covariance circular harmonic filters;
10. Wavelet matched filters.

We performed computer experiments using those algorithms. The conclusion of our investigation was that OFFMs are superior over other approaches. However, this method is computationally intensive and does not provide sufficient noise tolerance since high order moments are involved.

2.1 Orthogonal Fourier-Mellin Moments (OFMMs)

OFMMs are numerical features describing an image. OFMMs are scale, rotation, shift and intensity invariant. They are highly condensed image features, useful for image classification in feature space [2].

The advantage of this approach is that an image and all its rotated and scaled versions can be described and classified by a small number of OFMM features. The OFMMs provide a high degree of data compression. They are orthogonal. There is no information redundancy among the OFMM features.

The circular Fourier and radial Mellin transform (FMT) is defined in a polar coordinate system (r,θ) as

$$M_{s,m} = \int_0^{2\pi} \int_0^1 r^s \, f(r,\theta) \exp(-jm\theta) \, r \, dr \, d\theta \quad , \tag{2-1}$$

where $f(r,\theta)$ is the image and $m = 0, \pm 1, \pm 2, \ldots$ is the circular harmonic order. By definition, the Mellin transform of order s is complex. With integer $s \geq 0$, Eq. (2-1) defines the Fourier-Mellin moments (FMMs), also called the rotational moments. In the FMMs, the set of circular Fourier basis functions $\{\exp(-jm\theta)\}$ is orthogonal but the set of radial monomials $\{r^s\}$ is not orthogonal. The radial orders of the FMMs are highly correlated, resulting in information redundancy. To make the radial moments orthogonal, we replace the kernel function r^s of the FMMs by a set of polynomials $Q_n(r)$ in r of degree n. The set of $Q_n(r)$ is orthogonal with respect to a weight function r over the range $0 \leq r \leq 1$:

$$\int_0^1 Q_n(r) \, Q_k(r) \, r \, dr = a_n \, \delta_{nk} \quad , \tag{2-2}$$

where δ_{nk} is the Kronecker symbol, a_n is a normalization constant, and $r = 1$ is the maximum size of the objects that can be encountered in a particular application. The orthogonal radial polynomials rather than, for example, the Fourier transform basis are used, because the radial moments can be normalized to be invariant under scale changes, as will be shown below.

The orthogonal Fourier-Mellin moments (OFMMs) are defined as

$$\Phi_{nm} = \frac{n+1}{\pi} \int_0^{2\pi} \int_0^1 f(r,\theta)\, Q_n(r) \exp(-jm\theta)\, r\, dr\, d\theta \quad , \tag{2-3}$$

and are integrable when the degree of $Q_n(r)$, $n \geq 0$. The basis functions $Q_n(r)\exp(-jm\theta)$ of the OFMMs are orthogonal over the interior of the unit circle.

The orthogonal polynomials $Q_n(r)$ are obtained by applying the Schmidts process of orthogonalization to a sequence of natural powers of r over the range $0 \leq r \leq 1$

$$1, r, r^2, \ldots, r^n \quad . \tag{2-4}$$

By using Jacobi polynomials $G_n(p,q,r)$, we obtain the polynomials $Q_n(r)$ corresponding to the Jacobi polynomials with $p = q = 2$:

$$Q_n(r) = (-1)^n \binom{n+1}{n} G_n(2,2,r) = \sum_{s=0}^{n} \alpha_{ns}\, r^s \quad , \tag{2-5}$$

with

$$\alpha_{ns} = (-1)^{n+s} \frac{(n+s+1)!}{(n-s)!\, s!\, (s+1)!} \quad . \tag{2-6}$$

The normalization constant in Eq. (2-2) is $a_n = 1/[2(n+1)]$. The explicit expressions of $Q_n(r)$ are:

$$Q_0(r) = 1$$
$$Q_1(r) = -(2 - 3r)$$
$$Q_2(r) = 3 - 12r + 10r^2$$
$$Q_3(r) = -(4 - 30r + 60r^2 - 35r^3)$$
$$Q_4(r) = 5 - 60r + 210r^2 - 280r^3 + 126r^4$$
$$Q_5(r) = -(6 - 105r + 560r^2 - 260r^3 + 1260r^4 - 462r^5)$$
$$\ldots\ldots$$

Substituting Eqs. (2-1) and (2-5) into Eq. (2-3), we express the OFMMs as linear combinations of the FMMs

$$\Phi_{nm} = \frac{n+1}{\pi} \sum_{s=0}^{n} \alpha_{ns} \; M_{sm} \quad . \tag{2-7}$$

The OFMMs can be normalized to be invariant under rotation, scale, and intensity changes, as we will show below.

The FMMs and the OFMMs can also be defined in the Cartesian coordinate system as modified complex moments (CMs) and orthogonal CMs, respectively. This is important because, in most cases, images are presented in a Cartesian coordinate system. Calculating the OFMMs directly in the Cartesian coordinate system can avoid the coordinate transform of the image from the Cartesian to the polar coordinate system.

The orthogonal basis functions $Q_n(r) \exp(-jm\theta)$ of the OFMM can be expressed as complex polynomials in $(x + jy)$ and $(x - jy)$. The CMs are defined in both the Cartesian and the polar coordinate system [3]:

$$\begin{aligned} C_{pq} &= \int_{-\infty}^{\infty} \int f(x,y) \, (x + jy)^p \, (x - jy)^q \, dx \, dy \\ &= \int_{0}^{2\pi} \int_{0}^{1} f(r,\theta) \, r^s \, \exp\left(-jm\theta\right) r \, dr \, d\theta \end{aligned} \quad , \tag{2-8}$$

with $s = p + q$ and $m = q - p$. By the definition of Abu-Mostafa and Psaltis, the orders p and q are non-negative integers. From Eqs. (2-5) and (2-7),

$$Q_n(r) \exp(-jm\theta) = \sum_{s=0}^{n} \alpha_{n,s} \; r^s \; \exp(-jm\theta) = \sum_{s=0}^{n} \alpha_{n,s} (x + jy)^p \, (x - jy)^q \quad , \tag{2-9}$$

are a set of complex polynomials of degree $n = p + q$, where

$$p = \frac{s-m}{2} \qquad \text{and} \qquad q = \frac{s+m}{2} \quad , \tag{2-10}$$

orthogonal inside a unit circle. Hence, the OFMM can be expressed as a linear combination of the CMs as

$$\Phi_{nm} = \frac{n+1}{\pi} \sum_{s=0}^{n} \alpha \, C_{\frac{s-m}{2}, \frac{s+m}{2}}, \tag{2-11}$$

where the orders $\frac{s-m}{2}$ and $\frac{s+m}{2}$ of the CMs, C_{pq}, are real-valued and can be negative-valued. Under the conditions that both $p+q=s$ and $q-p=m$ are integers and $s=p+q \geq 0$, the modified CMs are convergent and integrable.

In the following experiments, the OFMMs will be calculated as the orthogonal CMs expressed in Eq. (2-11).

2.2 Procedure for Computing the OFMM Features

The steps in computing the OFMMs of an image follow.

1. Determine the center of the image by using the first order of the geometrical moments of the image:

$$x_0 = \frac{m_{10}}{m_{00}} \qquad y_0 = \frac{m_{01}}{m_{00}}, \tag{2-12}$$

where the geometrical moments m_{pq} are defined as

$$m_{pq} = \int_{-\infty}^{\infty} \int f(x,y)\, x^p\, y^q \, dx \, dy \; . \tag{2-13}$$

With the center of the image as the origin of the coordinate system, the moments calculated in this coordinate system would be shift invariant.

2. Calculate the FMMs, M_{sm}, defined in Eq. (2-1), by calculating the corresponding modified complex moments C_{pq} described in Eq. (2-8) with $p = \frac{s-m}{2}$ and $q = \frac{s+m}{2}$ in the Cartesian coordinate system;

3. Normalize the FMMs for the scale and illumination invariance. When the object $f(r,\theta)$ is scaled by a factor k and its intensity is changed by a factor g, its FMMs become

$$M'_{sm} = \int_0^{2\pi}\int_0^1 gf\,(r/k,\theta)\,r^s\,r\,dr\,d\theta = gk^{s+2}\,M_{sm} \quad . \tag{2-14}$$

The scale and intensity factors k and g are obtained using the low order FMMs:

$$\begin{aligned} M'_{00} &= gk^2\,M_{00} \\ M'_{10} &= gk^3\,M_{10} \end{aligned} \quad . \tag{2-15}$$

The scale factor k is equal to

$$k = \left(\frac{M'_{10}}{M'_{00}}\right) \Big/ \left(\frac{M_{10}}{M_{00}}\right) \quad . \tag{2-16}$$

The intensity factor g is equal to

$$g = \left[\left(\frac{M_{10}}{M_{00}}\right) \Big/ \left(\frac{M'_{10}}{M'_{00}}\right)\right]^2 \left(\frac{M'_{00}}{M_{00}}\right) \quad . \tag{2-17}$$

Using the factors k and g, the FMMs may be normalized as

$$M_{sm} = \frac{M'_{sm}}{gk^{s+2}} \quad . \tag{2-18}$$

The normalized FMMs are scale and intensity invariant.

4. Calculate the OFMMs using Eq. (2-7) and the normalized FMMs. A rotation of the image by an angle θ_0 results in the same phase factor $\exp(jm\theta_0)$ for all the M_{sm} in Eq. (2-7). The modulus of the OFMM, $|\Phi_{nm}|$, is rotation invariant.

4. Calculate the OFMMs using Eq. (2-7) and the normalized FMMs. A rotation of the image by an angle θ_0 results in the same phase factor exp ($jm\theta_0$) for all the M_{sm} in Eq. (2-7). The modulus of the OFMM, $|\Phi_{nm}|$, is rotation invariant.

2.3 Conclusions Regarding the Use of OFMMs

Although superior to other known STRI algorithms, OFMM-based ATR suffers from

- low noise tolerance (especially if it is introduced far from the center of the image frame)
- computational intensity (for a large number of moments)
- no optical (parallel processing) implementation.

3.0 PROOF OF STRI PREPROCESSING ALGORITHM

POC's proposed STRI ATR concept eliminates the main deficiencies of previous algorithms: the proposed algorithm is robust and noise tolerant and ready for optical implementation in a standard coherent optical system.

The proposed idea enhances existing optical correlation based ATR by introducing scale, translation and rotation invariance (STRI). Previously, STRI was achieved by utilizing a library of matching filters corresponding to various positions of rotation and scale. We find that simple preprocessing can eliminate the need for the library since any STR changes in the input image can be nullified by bringing the input image to, as we call it, its archetype. This means that any STR transformation of the target can be reduced to the initially defined target archetype. The archetype fully determines the whole class of STR transformed images of the given target.

This archetype image is characterized by the following features:

- Its center of gravity is coincident with a predetermined origin.
- It has a certain angle, specific to a given image, with the horizontal and vertical axes.
- It always has the same predetermined scale.

Translation invariance is achieved the same way as in moment transforms. Namely, for a given image I(x,y), the center of gravity (x_c, y_c) can be found by using the following expressions:

$$x_c = \frac{\iint_{\Omega} xI(x,y)dx\,dy}{\iint_{\Omega} I(x,y)dx\,dy}, \qquad y_c = \frac{\iint_{\Omega} yI(x,y)dx\,dy}{\iint_{\Omega} I(x,y)dx\,dy} \tag{3-1}$$

where Ω is the area of an input frame. The assumption is made that the input image is contained inside the input frame. Then, by shifting the input image by a vector $\begin{bmatrix} x_c \\ y_c \end{bmatrix}$,

$$\begin{cases} x' = x - x_c \\ y' = y - y_c \end{cases}, \tag{3-2}$$

we bring the image to the origin. (x',y') are the new coordinates of the image.

The most striking aspect of the proposed STRI concept is the rotation invariance property. In order to prove it, let us consider a function $\psi(\theta)$ that is obtained as a result of the integration of the input image in polar coordinates:

$$\psi(\theta_0) = \int_0^R \int_0^{2\pi} \cos\theta\, I(r, \theta - \theta_0)\, r d\theta\, dr, \tag{3-3}$$

where R is the radius of the smallest circle covering the input frame.

By changing the variable to $\varphi = \theta - \theta_0$ and using the formula for $\cos(\varphi + \theta_0)$,

$$\psi(\theta_0) = \cos\theta_0 \int_0^R \int_0^{2\pi} \cos\varphi\; I(r,\varphi)\, dr\, r d\varphi + \sin\theta_0 \int_0^R \int_0^{2\pi} \sin\varphi\; I(r,\varphi)\, r\, dr d\varphi \quad . \tag{3-4}$$

If we call the first double integral A and the second B, then the short-hand notation of Eq. (3-4) is

$$\psi(\theta_0) = A\cos\theta_0 - B\,\sin\theta_0 \quad , \tag{3-5}$$

or

$$\psi_0(\theta_0) = \cos\theta_0 \cos\alpha - \sin\theta_0 \sin\alpha = \cos(\theta_0 + \alpha) \ , \tag{3-6}$$

where

$$\cos\alpha = A/(A^2 + B^2)^{1/2} \ , \ \sin\alpha = B/(A^2 + B^2)^{1/2} \ , \ \psi_0 = \psi/(A^2 + B^2)^{1/2} \ . \tag{3-7}$$

Clearly, in the interval from 0 to 2π, $\psi_0(\theta_0)$ has a single minimum, $\psi_0(\theta_0) = -1$, which is achieved at

$$\theta_0 = \pi - \alpha \ , \tag{3-8}$$

regardless of the rotation of the input image. Thus, by computing the angle θ_0 ($0 \le \theta_0 \le 2\pi$) by

$$\theta_0 = \pi - \arctan(A/B) \ , \tag{3-9}$$

where

$$\begin{aligned} A &= \int_0^R \int_0^{2\pi} \cos\varphi \, I(r,\varphi) r \, dr \, d\varphi \\ B &= \int_0^R \int_0^{2\pi} \sin\varphi \, I(r,\varphi) r \, dr \, d\varphi \end{aligned} \ , \tag{3-10}$$

and rotating the input image by θ_0, the input image is brought to the archetypal angular position.

The last step is to normalize any changes in scale. This is achieved by computing the input image norm M:

$$M = \iint_\Omega I(x,y) dx \, dy \ , \tag{3-11}$$

and changing the coordinates by a scaling factor $\sqrt{M}$. This will assure that the input image will be normalized, regardless of its initial scale. Indeed, if the input image is zoomed by a factor c, then its new norm is

$$M_c = \iint_\Omega I(cx,cy) dx \, dy = M/c^2 \ , \tag{3-12}$$

and changing the coordinates by a scaling factor $\sqrt{M}$. This will assure that the input image will be normalized, regardless of its initial scale. Indeed, if the input image is zoomed by a factor c, then its new norm is

$$M_c = \iint_{\Omega} I(cx,cy)dx\,dy = M/c^2 , \tag{3-12}$$

and by changing the input image scale by a factor of $\sqrt{M_c}$, we again bring the image to the same scale

$$I(cx \cdot \sqrt{M_c}, cy \cdot \sqrt{M_c}) = I(x \cdot M, y \cdot M) , \tag{3-13}$$

which is an image archetype, since M is constant for a given image.

4.0 DIGITAL IMAGE ROTATION

The STRI transformation expressed by Eqs. (3-2), (3-9) and (3-12) has been successfully tested at POC.

POC's image-processing system consists of a Cohu CCD camera connected to a Matrox PIP video digitizer board installed in an IBM-compatible 486/66 personal computer. A black and white TV monitor was used to display the images. The image-processing station is shown in Figure 4-1. The digitizer board is supplemented with a library of C-language commands which were used to write the image-processing routines. The following is a summary of the tasks performed by these routines:

Figure 4-1
POC's image processing station.

First, the image of the object obtained by the CCD camera is digitized into a 256×256 array of 8-bit pixels. This image is then thresholded to set the background and shadows to zero. At this point, the center of gravity of the object is calculated with Eq. (3-1).

The object is then moved such that the center of the image area coincides with the center of gravity of the object. The translation accuracy has an error not larger than one pixel, which results from rounding up the numbers computed with Eq. (3-1).

The next task is to calculate the angle through which the object is to be rotated to reach its archetype. This angle, θ_0, is calculated with the following equation:

$$\theta_0 = \pi - \arctan(A/B)$$

where
$$A = \int_0^R \int_0^{2\pi} \cos\phi \, I(r,\phi) r \, dr \, d\phi \quad , \quad B = \int_0^R \int_0^{2\pi} \sin\phi \, I(r,\theta) r \, dr \, d\phi \quad . \tag{3-14}$$

The rotation task presents problems not associated with simple translation. Image rotation is a geometric process where one-to-one mapping of source to destination pixels is not guaranteed.

The rotation task presents problems not associated with simple translation. Image rotation is a geometric process where one-to-one mapping of source to destination pixels is not guaranteed. Without this one-to-one correspondence between source and destination pixels, it cannot be guaranteed that one source pixel will be mapped to every destination pixel. This creates voids that make the rotated images unusable. We employ reverse mapping to prevent these voids. Reverse mapping traverses the destination image space, a pixel at a time, and calculates, via the rotation transformation, which pixels of the source image would be involved in producing the destination pixel. When the value of the destination pixel is calculated in this manner and placed into the destination image, complete coverage of the destination image is guaranteed.

The other problem associated with rotation is that fractional pixel addresses may be calculated by the rotation transformation equations. This results in the calculated source image pixel lying somewhere between four valid pixel locations in the source image, again posing the problem of a lack of one-to-one pixel mapping. We first used the nearest neighbor approximation, where the fractional address of the source pixel is translated to the nearest integer pixel address. This, however, resulted in blocky and jagged images which were less than perfect. The solution to this problem was to use the interpolation method shown in Figure 4-2.

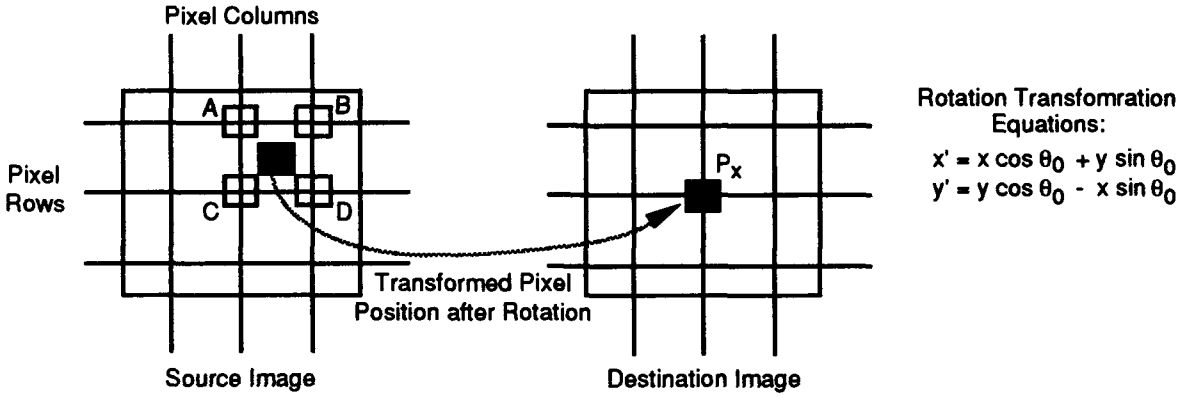

Figure 4-2
Interpolation method.

The four points surrounding the point being calculated (P_x) are referred to as the neighborhood. Linear interpolation assumes that the contribution of a pixel in the neighborhood varies linearly with its distance from a given point. Since we are interpolating in two dimensions, we perform three interpolations for the intensity contribution from pixels A and B, the contribution from pixels C and D, and the contribution from AB and CD.

The final problem associated with image rotation is the aspect ratio consideration. Because the TV monitor is not square, the pixels are not square. Rotation of nonsquare pixels results in distorted images. This problem was solved by using appropriate horizontal and vertical scale factors. The combination of reverse mapping, linear interpolation, and aspect ratio correction results in the best possible rotated images.

Two experiments were performed to test the operation of the image processing station. In the first experiment, the image of an object was thresholded, translated to the center, and rotated through its calculated characteristic angle. The original image of the object was then rotated through a random angle in the computer, and the resultant image was processed through the above routines. The two final images were compared and found to be identical. In the second experiment, the object was located in two different positions and the program brought it to its archetype position. This experiment also produced successful results.

5.0 EXPERIMENTAL PROOF OF STRI ALGORITHM

5.1 STRI Algorithm Demonstration

A set of 3-D objects, airplane models, was used to demonstration the STRI properties of the proposed algorithm (see Figure 5-1).

Figure 5-1
A set of models used for the STRI experiment.

For every model, 25 *arbitrary* STR transformations were performed and mean square errors (MSEs) were calculated for the resulting archetypes. The system (see Figure 4-1) operates in real-time. The results for two arbitrary target positions was displayed in less than 3 seconds.

The error for the two arbitrary STR transformed images as they are brought to the archetype position mainly occurs at the edges, as seen in Figure 5-2. Two randomly scaled images of the same model displaced from the center of the frame and rotated are shown at the top of the screen while one archetype (bottom left) and the difference between the two archetypes is shown at the bottom right of the screen.

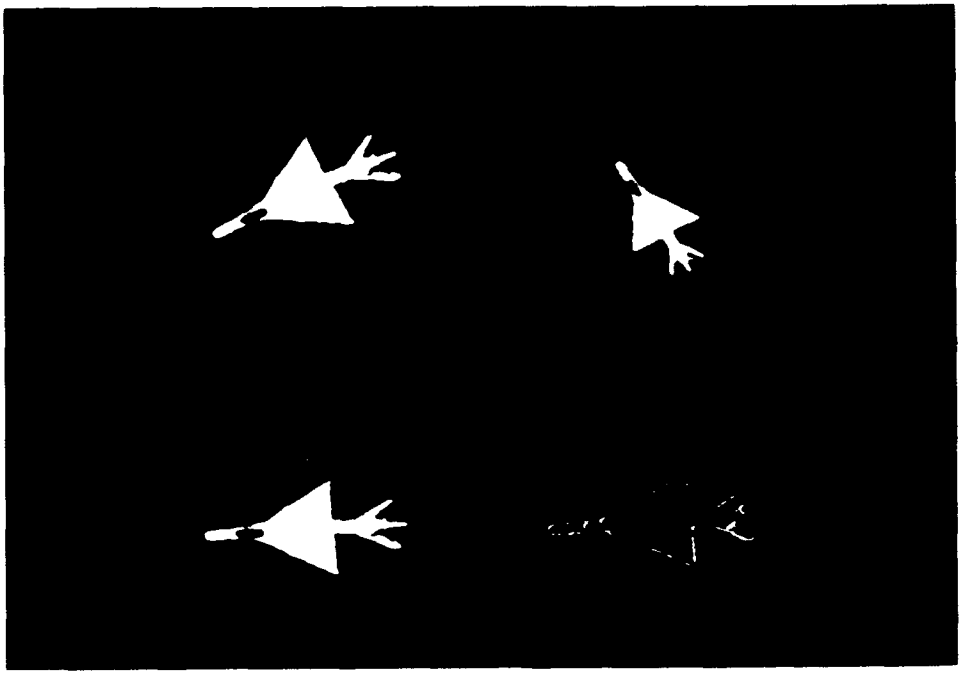

(a)

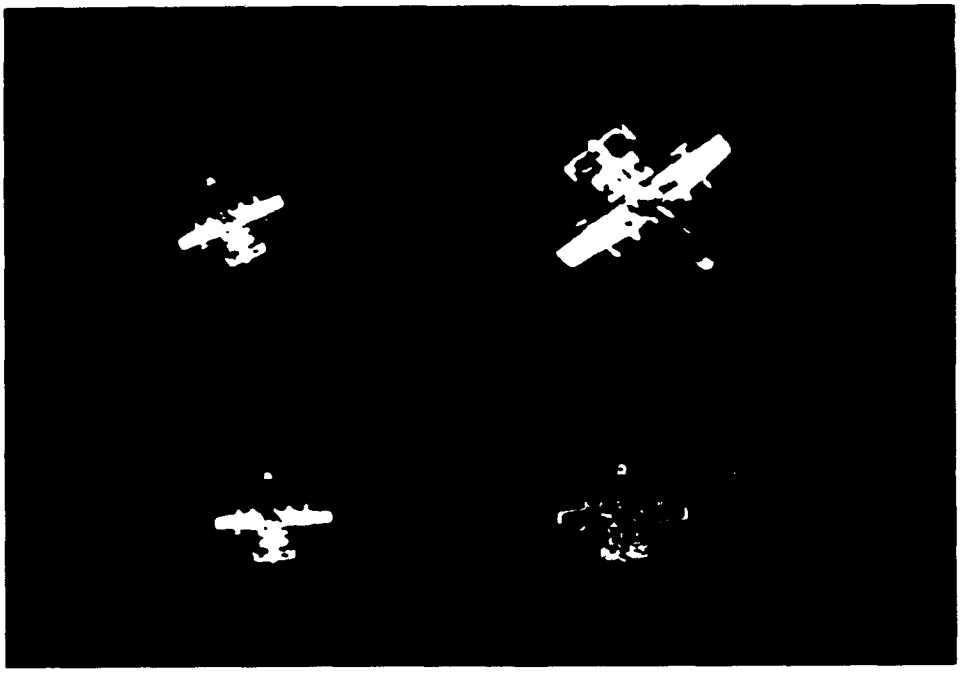

(b)

Figure 5-2
Example of STRI processing performed on two airplane models.

The MSE of the STRI processing for the four models shown in Figure 5-2 is summarized in Table 5-1. The processor demonstrated robust performance over a wide range of scale changes (300%), full 360° rotation, and all possible target translations within the image frame. The resulting archetypes are invariant and can be used to represent the whole class of the STR transformations of the object.

Table 5-1 MSE of STRI Processor

Model	MSE (%)
A	3.1
B	2.1
C	0.9
D	1.7

5.2 Noise Tolerance and Illumination Invariance

The STRI processor was tested for both noise tolerance and illumination invariance. Two low contrast objects (letters) were introduced into the imaged scene to stimulate additive external noise.

Figures 5-3 through 5-5 illustrate the fact that the STRI system can successfully operate under low contrast noise conditions. Each pair of photos shows the same model subjected to a random STR transformation and then returned to the same archetype position (shown in the insert). In addition, the images in Figure 5-6 were taken under different illumination conditions and the larger image is slightly out of focus.

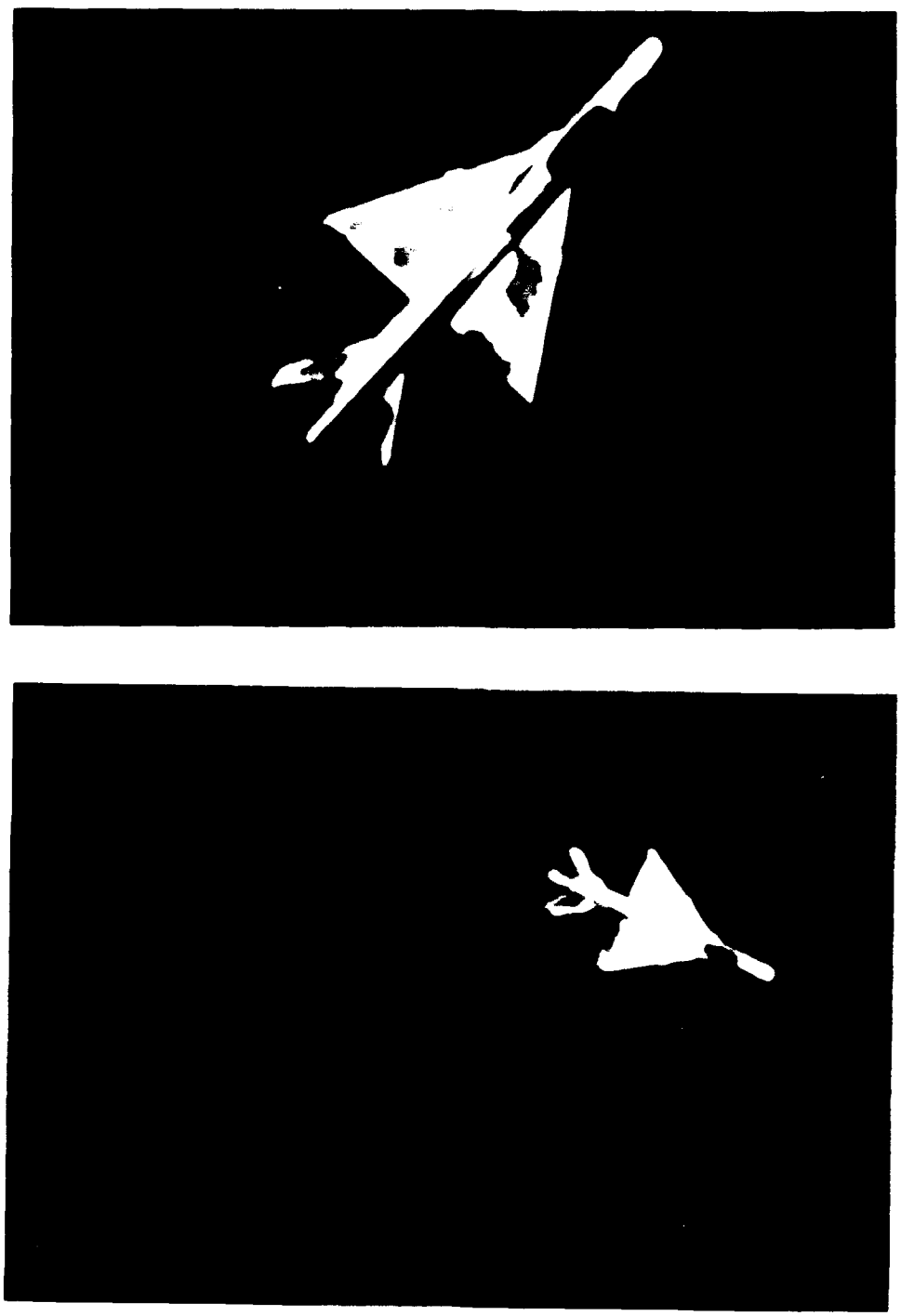

Figure 5-3
Performance of the STRI processor on an image scene with low contrast external noise. Model A is used here. The insert shows the system's reduction of the input model to the archetype.

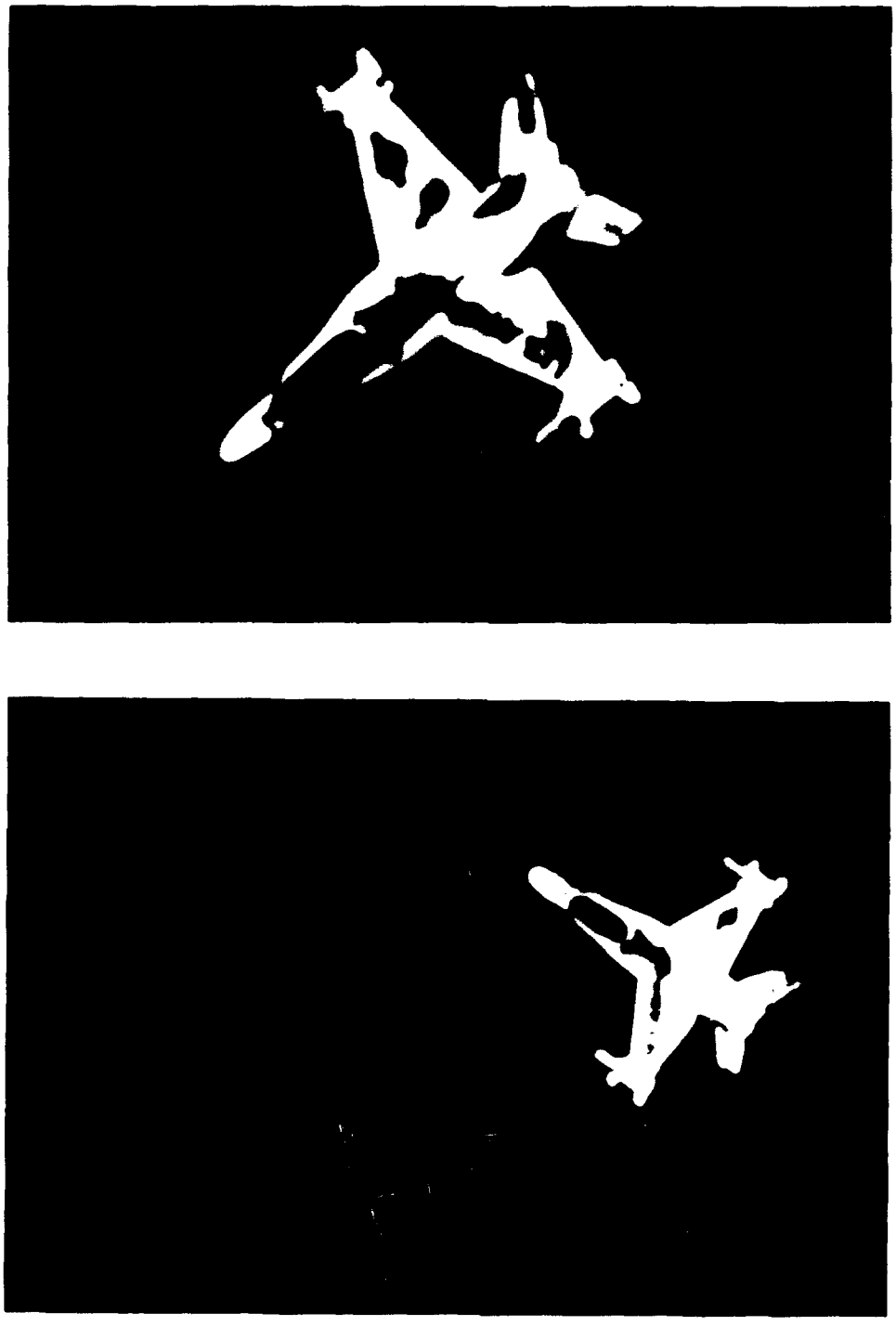

Figure 5-4
Same as Figure 5-3. Model C.

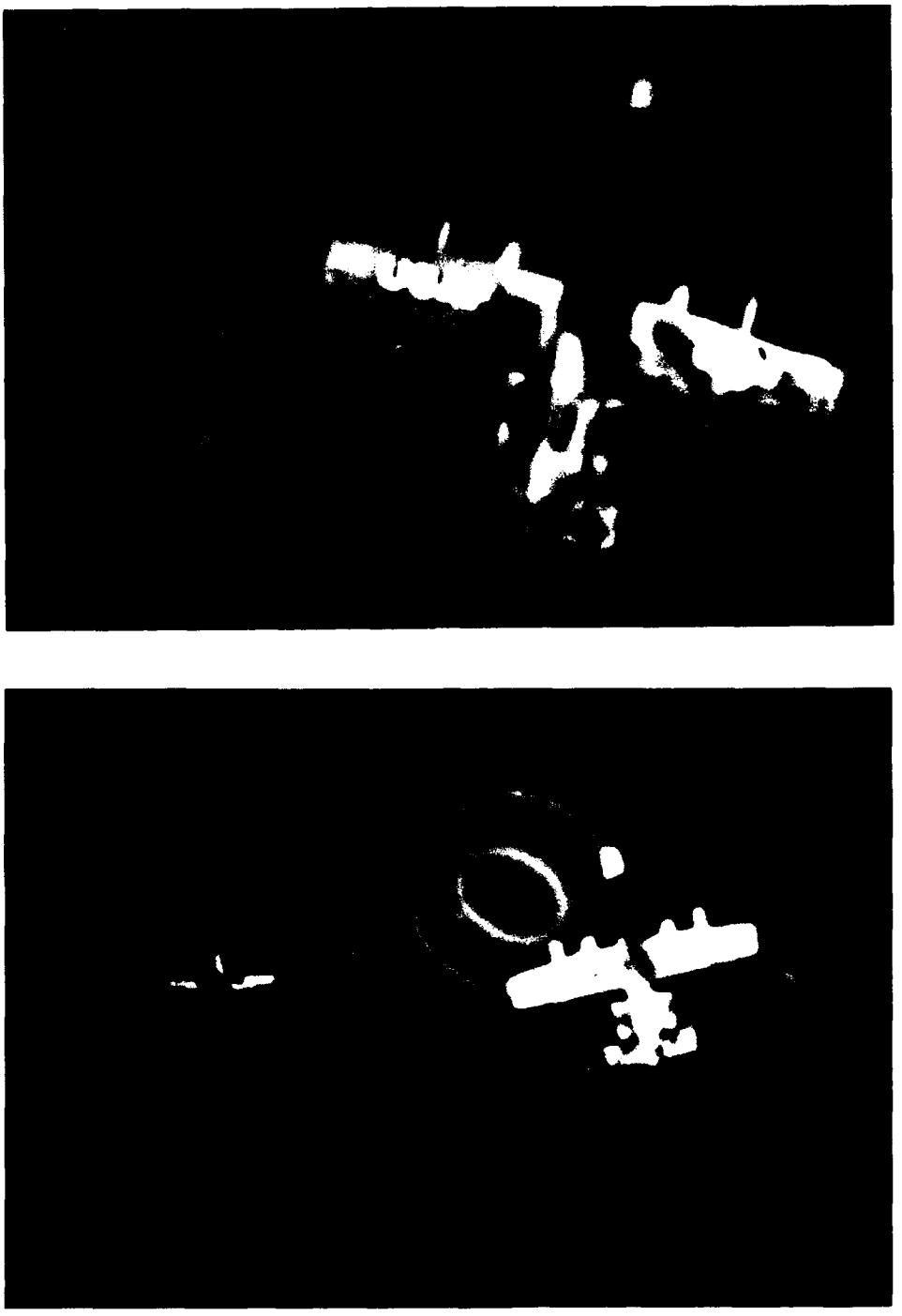

Figure 5-5
Same as Figure 5-3. Model B. In addition, the illumination level is different for the two images.

6.0 OPTICAL IMPLEMENTATION

The developed STRI digital processor can be used to supply an invariant image archetype as an input to an ATR system. Specifically, standard optical correlators fit very well with the STRI algorithm that has been implemented in the Phase I work. The schematic diagram of the resulting ATR system is shown in Figure 6-1.

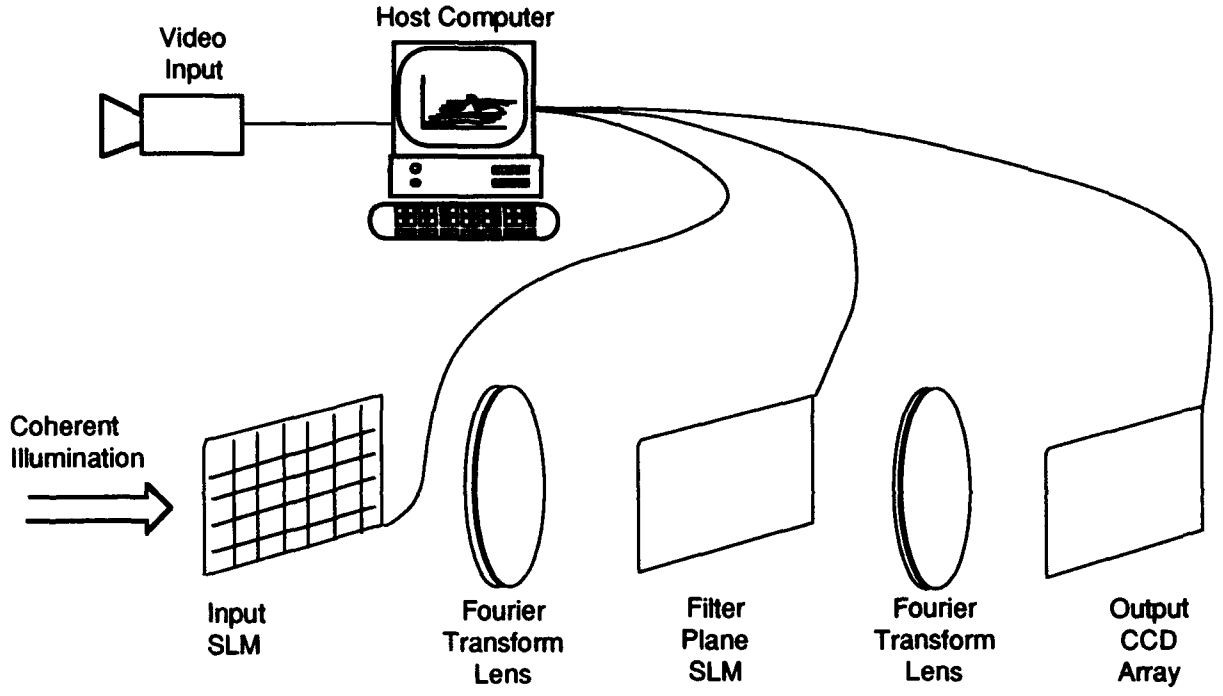

Figure 6-1
Schematic of the optical implementation of the STRI ATR system.

As was mentioned earlier, only one matched filter is needed for every target to accommodate all possible in plane STR transformations. This is in sharp contrast to the standard optical correlator where target rotations (typically of few degrees) and scale changes (usually larger than 5%) must be recorded as a separate matched filter (or combined into a synthetic filter). The photograph in Figure 6-2 shows a hardware implementation of an ATR system demonstrated at POC. For this system, the previously demonstrated digital processor operates as a preprocessor for the optical correlator. Since the matched filter for the archetype of the given target is recorded, any STR transformed image of the object will trigger the correlation, resulting in a strong correlation peak (see Figure 6-3). In this experiment, a DCG based matched filter accommodated a pair of targets

a pair of targets (Models B and C) through angular multiplexing. They were presented to the correlator using a liquid crystal spatial light modulator (SLM), as shown in Figure 6-4.

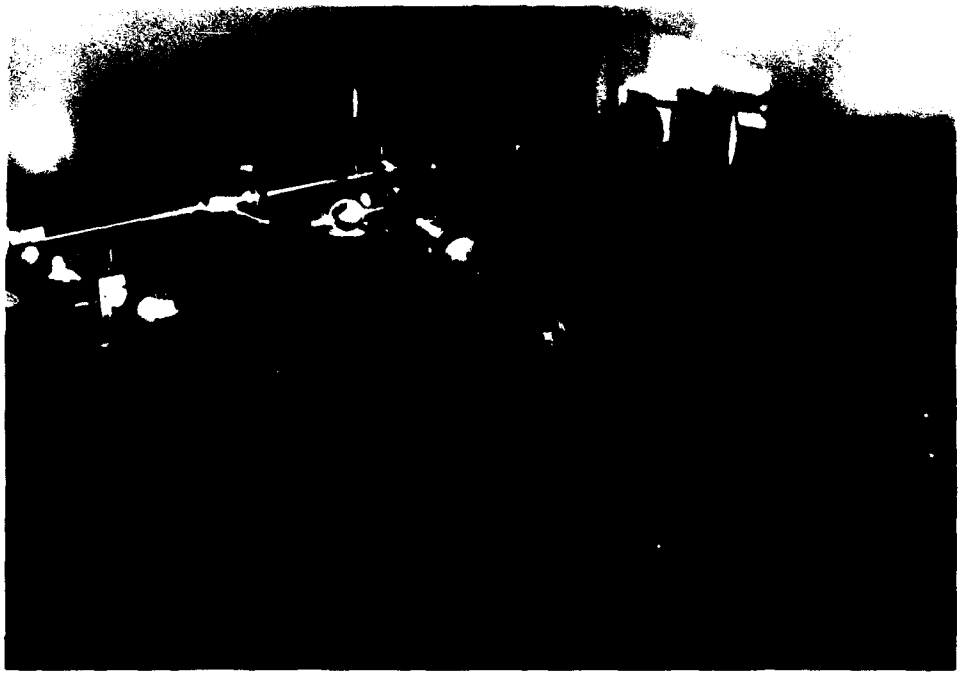

Figure 6-2
POC's correlator combined with the STRI preprocessor.

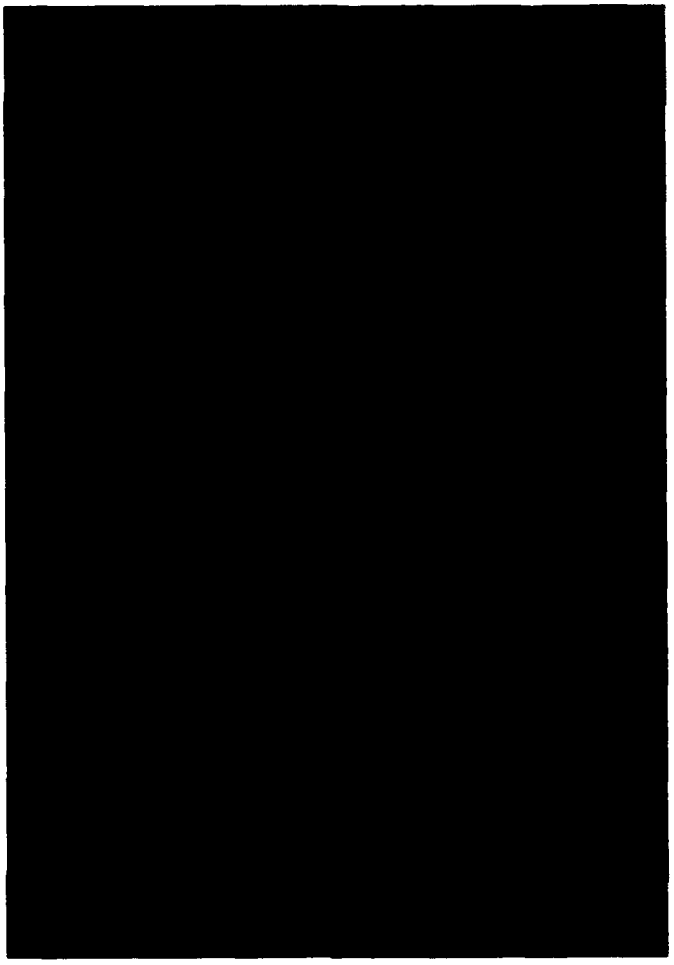

Figure 6-3
Auto correlation and cross correlation peaks observed at the system output.
(The bottom line seen on the oscilloscope is the intensity scan.)

Model B

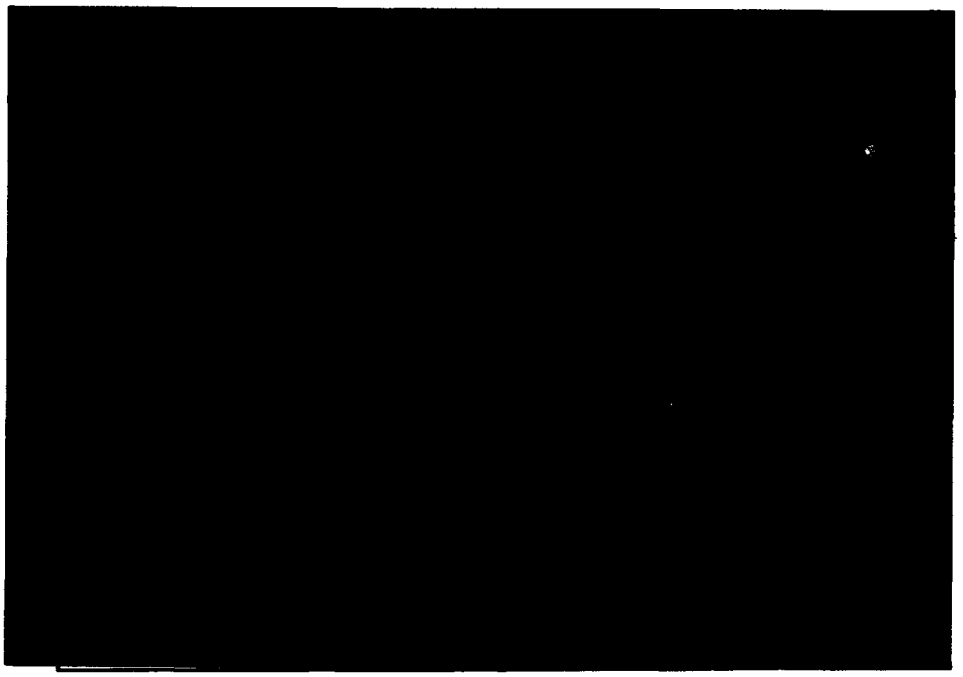

Model C

Figure 6-4
Images of the model as they appeared on the input SLM after preprocessing.

Then, the STR transformed images trigger the corresponding matched filter to produce a correlation output, as is seen in Figure 6-5. Thus, the preprocessor developed in this project makes the correlator fully STR invariant.

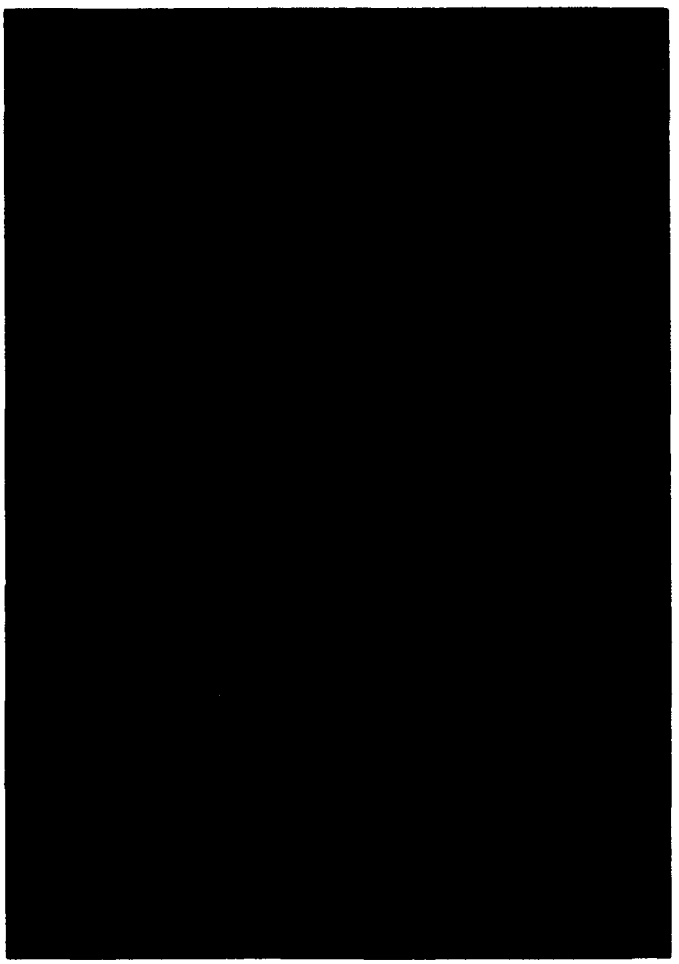

Figure 6-5
Correlation output from the multiplexed matched filter for the two targets shown in Figure 6-4.

7.0 CONCLUSION

The operating principle of the developed STRI system is summarized in the flow chart in Figure 7-1.

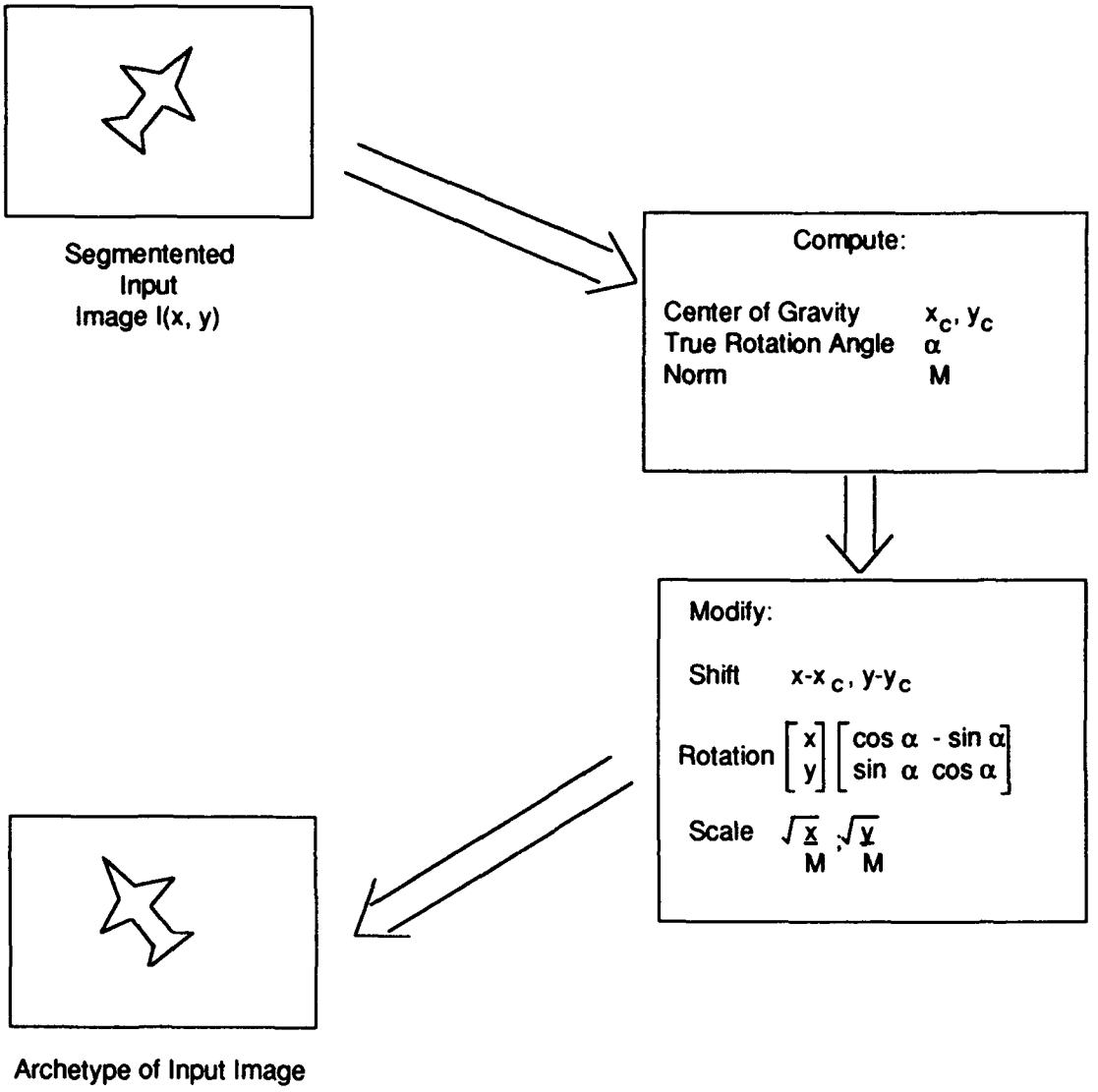

Figure 7-1
Diagram of STRI preprocessor operation.

The proposed concept is a significant step in the development of ATR systems, since it

- introduces complete factorization of the input space
- provides full (theoretically unlimited) STR invariance
- does not require computation of higher order moments which negatively affect noise tolerance
- minimizes matched filter loads.

8.0 PHASE II SUGGESTIONS

The proposed ATR system will use STRI wavelet transformation (WT) as a feature extractor and a neural network (NN) as a final classifier. The direct classification by the NN (without data compression) would fail because of the large number of input neurons required. This number equals the number of pixels in the input picture. The WT representation is an excellent candidate for data compression. However, in order to accommodate all possible STR transformations, the NN should store a very large number of weight matrices corresponding to every distinct target pose. This again makes this approach less practical. The STRI feature extractor allows the whole class of STR transformations of the given target to be represented by a single set of wavelet coefficients. It greatly reduces the NN classifier's load. The proposed ATR system can be practically implemented following the diagram in Figure 8-1. While image acquisition and preprocessing use existing hardware and software, the innovative part of the proposed ATR system is the STR invariant WT feature extractor. Notice that we do not perform any transformation on the input image. In the digital implementation of the STR invariant WT concept, we need only compute values of the new basic wavelet functions at the nodes of the old pixel grid. Starting from an analytical expression for the new function, our feature extractor preserves all the information given in the input image and involves no additional approximation error.

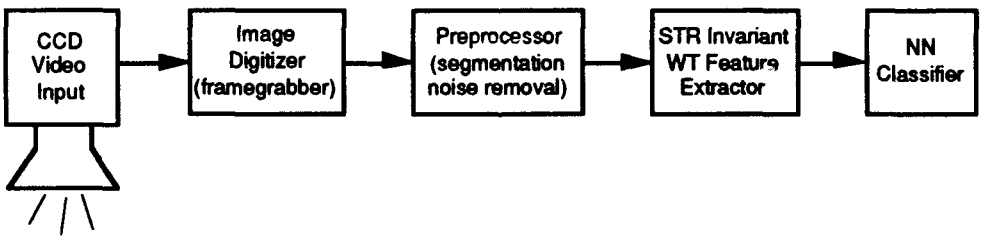

Figure 8-1
STR invariant WT for ATR.

9.0 REFERENCES

1. A. Vander Lugt, "Signal Detection by Complex Spatial Filter," IEEE Trans., IT-10, pp. 139-148 (1964).

2. Y. Sheng and L. Shen, "Orthogonal Fourier-Mellin Moments for Invariant Pattern Recognition," submitted to JOSA A (1993).

3. Y. S. Abu-Mostafa and D. Psaltis, "Recognition Aspect of Moment Invariants," IEEE Trans. Pattern Anal. and Mach. Intell., **PAMI-6**, 698-706 (1984).